



HAL
open science

Nonlinear repolarization dynamics in optical fibers: transient polarization attraction

Victor V. Kozlov, Julien Fatome, Philippe Morin, Stéphane Pitois, Guy
Milot, Stefan Wabnitz

► **To cite this version:**

Victor V. Kozlov, Julien Fatome, Philippe Morin, Stéphane Pitois, Guy Millot, et al.. Nonlinear repolarization dynamics in optical fibers: transient polarization attraction. *Journal of the Optical Society of America B*, 2011, 28 (8), pp.1782-1791. 10.1364/JOSAB.28.001782. hal-00638973

HAL Id: hal-00638973

<https://hal.science/hal-00638973>

Submitted on 7 Nov 2011

HAL is a multi-disciplinary open access archive for the deposit and dissemination of scientific research documents, whether they are published or not. The documents may come from teaching and research institutions in France or abroad, or from public or private research centers.

L'archive ouverte pluridisciplinaire **HAL**, est destinée au dépôt et à la diffusion de documents scientifiques de niveau recherche, publiés ou non, émanant des établissements d'enseignement et de recherche français ou étrangers, des laboratoires publics ou privés.

Nonlinear repolarization dynamics in optical fibers: Transient polarization attraction

V. V. Kozlov^{1,2,*}, J. Fatome³, P. Morin³, S. Pitois³, G. Millot³, and S.

Wabnitz¹

¹*Department of Information Engineering, Università di Brescia,*

Via Branze 38, 25123 Brescia, Italy

²*Department of Physics, St.-Petersburg State University,*

Petrodvoretz, St.-Petersburg, 198504, Russia

³*Laboratoire Interdisciplinaire Carnot de Bourgogne (ICB), UMR 5209 CNRS /*

Université de Bourgogne 9 av. Alain Savary, 21078 Dijon, France

**Corresponding author: victor.kozlov@email.com*

In this work we present a theoretical and experimental study of the response of a lossless polarizer to a signal beam with a time-varying state of polarization. By lossless polarizer we mean a nonlinear conservative medium (e.g., an optical fiber) which is counter-pumped by an intense and fully polarized pump beam. Such medium transforms input uniform or random distributions of the state of polarization of an intense signal beam into output distributions which are tightly localized around a well defined state of polarization. We introduce and characterize an important parameter of a lossless polarizer – its response time. Whenever the fluctuations of the state of polarization of the input signal beam are slower than its response time, a lossless polarizer provides an efficient re-polarization of the beam at its output. Otherwise if input polarization fluctuations are faster than the response time, the polarizer is not able to re-polarize light. © 2011 Optical Society of America

OCIS codes: 230.5440 Polarization-selective devices; 060.4370 Nonlinear optics, fibers; 230.1150 All-optical devices; 230.4320 Nonlinear optical devices

1. Introduction

Over the last few years there has been a great deal of interest in the development of polarization-selective devices for nonlinear optics and telecom applications. The simplest and most common way to select a desired polarization state out of a laser source or from a telecom link is to insert a linear polarizer. A linear polarizer transmits only

one polarization state and rejects all others. Clearly a constant intensity, but polarization fluctuating beam may acquire large intensity fluctuations after passing through a linear polarizer, possibly resulting in significant degradation of the signal-to-noise ratio after detection. In addition, polarization-dependent losses may be detrimental when using nonlinear optical devices. In this work we study the nonlinear lossless polarizer (NLP), a device which transforms all (or most) polarizations of the input beam into approximately one and same state of polarization (SOP) at its output, without introducing any polarization-dependent losses.

Three types of NLPs for controlling the light SOP have been proposed so far. Historically the first lossless polarizer was proposed and experimentally demonstrated in Ref. [1], where the effect of two-wave mixing in a photorefractive material was used for the amplification of a given polarization component of a light beam by using the orthogonal component as a pump beam. However the use of such device in telecommunication applications is limited by the intrinsically slow (of the order of seconds and minutes) response time inherent to photorefractive crystals. In this respect, it appears that NLPs based on the Kerr nonlinearity of optical fibers are more promising for fast SOP control. Indeed, a fiber-based NLP was experimentally demonstrated in a practical configuration involving a 20 km long, low polarization-mode dispersion telecom (randomly birefringent) fiber, counter-pumped with a 600 mW continuous wave (CW) beam (Ref. [2]). This NLP was able to smooth at its output microsecond-range polarization bursts of the input 300 mW signal beam. A recent theoretically study has

analyzed the CW operation of a NLP in the presence of random fiber birefringence Ref. [3]. The third type of lossless polarizers are also based on a Kerr medium, but do not require a counter-propagating beam. Here the spontaneous polarization which is induced by natural thermalization of incoherent light in the nonlinear medium lies at the heart of the repolarization mechanism, see Ref. [4].

In this paper we devote our attention to the second class of NLPs. Their principle of operation is based on the so-called polarization attraction effect: virtually any input SOP of the signal beam is attracted to the vicinity of a definite SOP towards the device output. When visualized on the Poincaré sphere, all SOPs that are initially randomly (or uniformly) distributed over the entire Poincaré sphere contract into a small well-localized spot. The size of this spot, which is measured in terms of the degree of polarization (DOP) D

$$D = \frac{1}{S_0} \sqrt{\sum_{i=1}^3 \langle S_i \rangle^2}. \quad (1)$$

(the smaller the size, the higher the DOP), quantifies the performance of a NLP. In Eq. (1)) the average of the Stokes parameters that describe the state of polarization of a beam is performed as either a time or an ensemble average, as discussed in details in section 3. A practically relevant question involves the choice of the nonlinear fiber. Historically, the first fiber-based NLP was realized in isotropic fibers, see Ref. [5, 6]. The disadvantage of this setup is in the necessity to use high-power (~ 50 W) beams

in order to obtain the efficient nonlinear interaction of two counter-propagating beams over only highly nonlinear one-two meter long fiber span (for the corresponding theory see Refs. [8–11]). A bold step forward towards the practical use of these devices was provided by the recent experimental demonstration of lossless polarization attraction in a 20-km long telecommunication fiber: such configuration permits for two orders of magnitude reduction in the pump (and signal) power, Ref. [2]. This solution is versatile, cheap, and easily integrable with most optoelectronic devices. As theoretically demonstrated in Ref. [7], lossless polarizers can be also implemented with a relatively shorter (~ 100 m) sample of highly nonlinear high birefringent or unidirectionally spun fiber.

The theoretical model presented in Ref. [3] unites all types of fibers (isotropic, deterministically birefringent, randomly birefringent, and spun) under one umbrella by showing that the propagation of counter-propagating beams in silica fibers is described by the same evolution equations: different fibers lead to specific values of the coefficients entering these equations. Fiber based NLPs have different performances, but all exhibit the effect of polarization attraction under similar conditions of operation. Driven by practical considerations, we choose to work here with a telecommunication (i.e. randomly birefringent) fiber. Although so far the most studied case involves isotropic fibers, the theory which has been developed for these fibers cannot be directly applied to telecommunication fibers for the reasons to be discussed over the next sections.

The literature available so far on telecommunication fiber-based NLPs, see Refs. [2, 3], was mainly aiming at the proof-of principle experimental and theoretical demonstration of the polarization attraction effect. Here we set our goal in substantially extending these results by characterizing through both numerical simulations as well as experiments the temporal polarization dynamics of NLPs. In section 2 we formulate the model for the interaction of time-varying, counterpropagating beams in a randomly birefringent optical fiber, and provide the definition of the response time of a NLP. In section 3 we provide first the definition of the two types of input signals that will be considered in this work, namely input unpolarized light or scrambled light. In section 3.A we analyze the temporal response of the NLP to an input polarized beam, and reveal the possibility of obtaining periodic or even irregular temporal oscillations of the output SOP in correspondence of a CW input beam. Next in section 3.B we present extensive numerical simulations where we compare ensemble and temporal averaging of the output SOP in the presence of either scrambled or unpolarized signals, respectively. We show that whenever the time variations of the input unpolarized light are slow with the respect to the NLP response time, the repolarization by the NLP is ergodic in the sense that ensemble and time averages lead to virtually identical results. However this property no longer holds as the time variation of the input unpolarized light is faster than the response time: in this situation, the repolarization property of the NLP no longer holds. In order to further investigate this point, we have numerically and experimentally investigated in sections 3.A and

4 the repolarization action of a NLP upon a short input polarization fluctuation (or burst), as a function of the relative duration of the burst with respect to the response time. Simulations and experiments demonstrate with excellent agreement that uniform repolarization by the NLP requires polarization burst durations longer than the NLP response time. A discussion and conclusion is finally presented in section 5.

2. Model Equations

The formulation of a model for describing the interaction of two counterpropagating and arbitrarily polarized beams in a Kerr medium with randomly varying birefringence in terms of deterministic coupled differential equations is not a trivial task. Indeed such formulation requires the accurate evaluation of statistical averages, and it involves a number of assumptions. In our approach we make two main assumptions. The first hypothesis is that, among the two characteristics of the birefringence when represented as a three-dimensional vector, namely its magnitude and its orientation, the magnitude is fixed at a constant value along the total fiber length L . On the other hand we suppose that the orientation varies randomly with distance, with a characteristic correlation length L_c . The second assumption is that the fiber length $L \gg L_c$.

Based upon these two assumptions, one obtains a system of differential equations with variable coefficients for describing the mutual polarization coupling of two counterpropagating waves [3]. We may argue that, in order to obtain a significant polar-

ization effect, the differential beat length $L'_B \equiv [L_B^{-1}(\omega_s) - L_B^{-1}(\omega_p)]^{-1}$ should obey the inequality $L'_B \gg L$, where $L_B(\omega_s)$ [$L_B(\omega_p)$] is the beat length at the signal (pump) frequency ω_s (ω_p). In fact, if the previous inequality is not satisfied, then the polarizations of the two beams are scrambled by linear birefringence before significant nonlinear attraction may take place. In the limit $L/L'_B \rightarrow 0$ the polarization coupling coefficients are no longer variable, and we are left with a set of equations with constant coefficients. These equations are conveniently formulated in Stokes space as

$$\partial_\xi \mathbf{S}^+ = \mathbf{S}^+ \times J_s \mathbf{S}^+ + \mathbf{S}^+ \times J_x \mathbf{S}^-, \quad (2)$$

$$\partial_\eta \mathbf{S}^- = \mathbf{S}^- \times J_s \mathbf{S}^- + \mathbf{S}^- \times J_x \mathbf{S}^+. \quad (3)$$

For details of the derivation see Ref. [3]. Here $\xi = (vt + z)/2$ and $\eta = (vt - z)/2$ are propagation coordinates, where v is the phase speed of light in the fiber. The sign "×" denotes vector product. The above equations are written for the three components $S_1^\pm = \phi_1^{\pm*} \phi_2^\pm + \phi_1^\pm \phi_2^{\pm*}$, $S_2^\pm = i(\phi_1^{\pm*} \phi_2^\pm - \phi_1^\pm \phi_2^{\pm*})$, and $S_3^\pm = |\phi_1^\pm|^2 - |\phi_2^\pm|^2$ of the signal $\mathbf{S}^+ = (S_1^+, S_2^+, S_3^+)$ and the pump $\mathbf{S}^- = (S_1^-, S_2^-, S_3^-)$ Stokes vectors, respectively. Here $\phi_{1,2}^\pm$ are the polarization components of the signal and pump fields in the chosen reference frame. Self- and cross-polarization modulation (SPM and XPM) tensors are both diagonal and have the form $J_s = \gamma_{ss} \text{diag}(0, 0, 0)$ and $J_x = \frac{8}{9} \gamma_{ps} \text{diag}(-1, 1, -1)$. Note that the condition $L'_B \gg L$ implies that the carrier wavelengths of the pump and signal beams are close to each other (i.e., their wavelength spacing does not exceed ~ 1 nm). Therefore, $\gamma_{ss} \approx \gamma_{ps} \approx \gamma$ where γ denotes the nonlinear coefficient.

Note that in our model the second and higher order group velocity dispersions are not taken into account for the reason that the pump and signal beams are considered as quasi-CWs. In other words, temporal modulations of the signal SOP beam are supposed to be relatively slow, so that dispersive effects can be neglected over the distances involved in our study.

For each beam we define the zeroth Stokes parameters S_0^+ and S_0^- according to the equation

$$S_0^\pm = \sqrt{(S_1^\pm)^2 + (S_2^\pm)^2 + (S_3^\pm)^2}. \quad (4)$$

These parameters represent the power of the forward and backward beams, respectively. Since we are dealing with wave propagation in a lossless medium, the sum of the powers of both beams is a conserved quantity along the fiber length. Moreover, the equations of motion (2) and (3) imply that the powers of each beam are separately conserved: $S_0^+(z - ct) = S_0^+(z = 0, t)$ and $S_0^-(z + ct) = S_0^-(z = L, t)$ for all z .

Henceforth we shall be dealing only with uniform (i.e. independent of z) initial conditions. These are related to the boundary conditions at $t = 0$ as follows

$$S_i^+(z = 0, t) = S_i^+(z, t = 0), \quad (5)$$

$$S_i^-(z = L, t) = S_i^-(z, t = 0). \quad (6)$$

with $i = 1, 2, 3$. The choice of the initial conditions only influences the short-term polarization evolutions of the two beams, as they have no influence on the long-term behavior of the polarization states. It is precisely such long-term evolution which is of

interest to us. Therefore from now on we shall only specify the boundary conditions: for the initial conditions we may refer to the previous relationships (5) and (6).

Let us also introduce the nonlinear length $L_{NL} = (\gamma S_0^+)^{-1}$, which has the meaning of the characteristic length of nonlinear beam evolution inside the fiber. In its turn, the characteristic time is simply defined as $T_{NL} = L_{NL}/v$. In our simulations we use L_{NL} as the unit for measuring distances in the fiber medium in a reference frame with the origin ($z = 0$) at the left boundary, where we set the boundary conditions for the forward (signal) beam. At the right boundary (i.e., at $z = L$) we set the boundary conditions for the backward (pump) beam. The temporal scale in units of T_{NL} is used for measuring time. In simulations to be carried out in the next section, we set the total fiber length equal to $L = 5L_{NL}$. We varied the pump power in the range $[1, 5.5]S_0^+$. Whenever the pump power drops below S_0^+ the effect of polarization attraction quickly degrades, therefore the power range $[0, 1]S_0^+$ is not of interest here.

3. Numerical simulations

In the numerical study of polarization attraction two different approaches can be distinguished. The first approach is the study of the response of the polarizer to input scrambled beams. By scrambled beams we understand a set of N beams, where each individual beam is fully polarized but the ensemble of the N SOPs is randomly or uniformly distributed over the entire Poincaré sphere. So, the DOP of the ensemble of beams is exactly zero. In this case we compute the SOP of the outcoming signal beam,

after its interaction with the nonlinear fiber pumped by the backward-propagating beam. We performed the integration of Eqs. (2)-(3) based on the numerical method which was proposed in Ref. [12]. The outcoming set of SOPs are averaged, as explained in Appendix A, so that the mean SOP and the DOP can be obtained. The repolarization property of the polarizer leads then to an output DOP which is different from zero. Note that the repolarization quality of the NLP depends on the specific polarization of the pump beam. In Ref. [3] we considered a set pump beam SOPs which are represented on the Poincaré sphere by points in the vicinity of its six poles, namely $(\pm 1, 0, 0)$, $(0, \pm 1, 0)$ and $(0, 0, \pm 1)$. We observed that in the last two cases the NLP works relatively better than in the first four cases. However the basic features of the polarization attraction do not critically depend on the choice of the pump SOP (even though significant variations in the output signal DOP may result when the pump SOP is varied). Therefore in the following simulations we will restrict our attention for simplicity to the case of a pump SOP equal to $(0.99, 0.1, 0.1)$. In this case the signal SOP is on average attracted to a point in the vicinity of the pole $(-1, 0, 0)$.

This approach permits to calculate the average response of the polarizer to any signal SOP in the stationary regime. That is, we obtain the output SOP long after that all transient processes have died away. The studies of NLPs that were undertaken in Refs. [3, 7] are based on this approach, which we term Approach S (scrambled).

An alternative approach involves the study of the response of a NLP to unpolarized

light. By unpolarized light we mean a beam whose the SOP is randomly varying in time on the scale of some characteristic correlation time T_c . Whenever the observation time T largely exceeds T_c , so that the coverage of the Poincaré sphere by the beam's SOP is uniformly covered, then the (time-averaged) DOP is also zero. In this paper we develop this approach and call it Approach U (unpolarized).

In the Approach S we perform the ensemble average, while in the Approach U we perform a time average. If these two statistical approaches yield identical results, then we may say that the system is ergodic. The numerical verification of the ergodicity of a NLP is the goal of the next subsection.

3.A. Response to polarized light

An ultimate goal of our simulations is to characterize the response of a NLP to a signal beam whose SOP is modulated in time with a characteristic frequency ω_m , thus mimicking the statistics of unpolarized beam. The three Stokes parameters of the input signal beam are specified by the two angles α_1 and α_2 (which define the position of the tip of the Stokes vector on the Poincaré sphere) as follows

$$S_1^+(z = 0, t) = S_0^+ \sin \alpha_1(t) \cos \alpha_2(t), \quad (7)$$

$$S_2^+(z = 0, t) = S_0^+ \sin \alpha_1(t) \sin \alpha_2(t), \quad (8)$$

$$S_3^+(z = 0, t) = S_0^+ \cos \alpha_1(t). \quad (9)$$

We choose to vary these angles in time according to the linear law

$$\alpha_1 = \alpha_0 + 2.53\omega_m t, \quad (10)$$

$$\alpha_2 = \alpha_0 - 3.53\omega_m t. \quad (11)$$

For observation times $T \gg \omega_m^{-1}$, it can be easily verified that the tip of the input Stokes vector almost uniformly covers the entire Poincaré sphere. Indeed for $T = 50\omega_m^{-1}$ the time-averaged input beam DOP is as low as 0.0074, which is low enough to consider the beam as virtually unpolarized.

Before coming to the consideration of input unpolarized beams, we find it instructive to treat the response of the NLP to fully polarized light: we may set for example $\omega_m = 0$ and $\alpha_0 = \pi/4$. First of all, let us observe the signal SOP at the fiber output medium (at $z = L$) as a function of time. After a short transient process, we observed that the Stokes vector components enter a regime of fully periodic oscillations, as demonstrated in Fig. 1. Depending on the input SOP, these temporal oscillations may have larger or smaller amplitude. For some input SOPs we observed a time stationary output. No other (for instance, chaotic, as earlier reported in the case of isotropic fibers, see Ref. [13]) regimes were detected at least for the limited range of pump and signal powers considered here. Also note that, as expected and in spite of the oscillations, the tip of the output signal SOP is on average attracted to a point which is located in the vicinity of the pole $(-1, 00)$.

Fig. 2 illustrates spatial distributions along the fiber length of the Stokes compo-

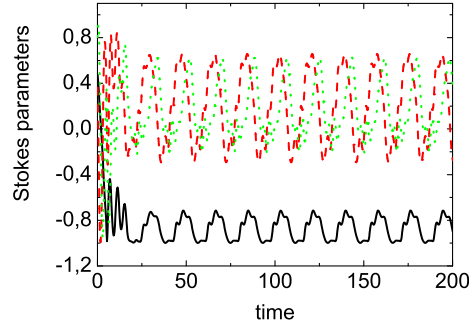


Fig. 1. Stokes parameters of the signal beam at $z = L$ as a function of time: S_1^+ (black solid); S_2^+ (red dashed); S_3^+ (green dotted). Time is measured in units T_{NL} . Stokes parameters are normalized to S_0^+ ; $S_0^- = 3S_0^+$.

nents of the signal at four successive times. Here we consider the same parameters that were used for generating Fig. 1. The four snapshots in Fig. 2 exactly cover one period of the temporal oscillations in Fig. 1. Indeed the time step between the snapshots is $\Delta t = 6T_{NL}$: the first snapshot is taken at $t = 30T_{NL}$ and the last at $t = 48T_{NL}$. Fig. 2 demonstrates how the Stokes components “breathe” all across the fiber except for the input end, where the state of polarization is clamped by the imposed stationary boundary conditions.

The period of oscillations of the Stokes parameters decreases with larger pump power as demonstrated in the left panel of Fig. 3. The periodic regime suddenly starts at $S_0^- = 1.9S_0^+$ (for our particular choice of signal and pump SOPs): below this pump power value the polarization evolution regime is purely stationary. We may

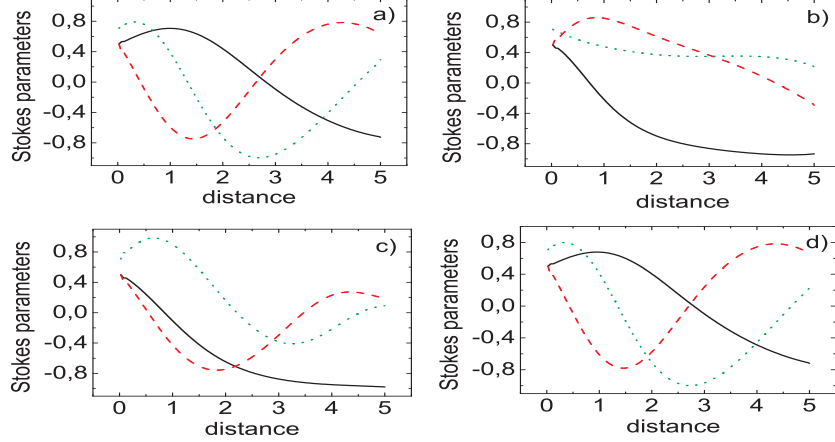


Fig. 2. Stokes parameters of the signal beam inside the medium at four instants of time: a) $t = 30$; b) $t = 36$; c) $t = 42$; d) $t = 48$. S_1^+ (black solid); S_2^+ (red dashed); S_3^+ (green dotted). Time is measured in units T_{NL} . All Stokes parameters are normalized to S_0^+ . Parameters are as in Fig. 1. The four snapshots cover exactly one period of the oscillations that are shown in Fig. 1.

argue that the system experiences a Hopf bifurcation: however a detailed study of the bifurcation diagram by methods of nonlinear dynamics is beyond the scope of this paper.

The practical consequence of the periodic temporal oscillations of the Stokes parameters for pump power larger than $1.9S_0^+$ is the depolarization of the signal at the fiber output end. In the specific case discussed here, an input fully polarized beam with $\text{DOP} = 1$ transforms into an output partially polarized beam with $\text{DOP} = 0.9$,

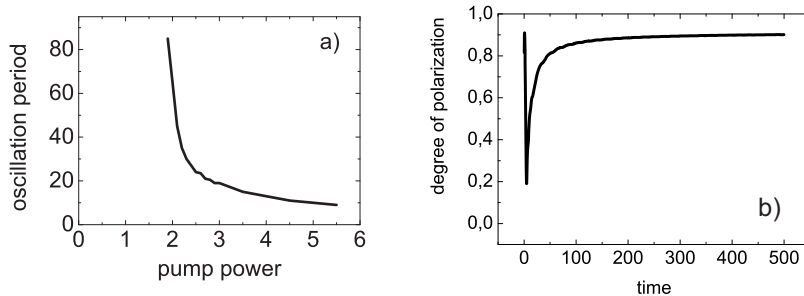


Fig. 3. (a): Period (in units of T_{NL}) Stokes parameter oscillations at $z = L$ versus pump power (in units of S_0^+); (b) DOP versus time for the same case as in Figs. 1 and 2.

as demonstrated in the right panel of Fig. 3. Here the DOP is calculated as

$$D_U(T) = \frac{1}{T} \frac{1}{S_0^+} \sqrt{\sum_{i=1}^3 \left[\int_0^T dt S_i^+(L, t) \right]^2}. \quad (12)$$

Here the index U associated to time average (over a time interval T much larger than T_{NL}) which is characteristic of the previously defined Approach U. In situations where larger amplitude oscillations of the state of polarization of the output signal occur, the corresponding DOP is further reduced and may in principle even drop below 0.1, as we shall see in the next subsection. From these observations we deduce a rather unexpected behavior for a polarizer: namely, it transforms a fully polarized beam into a partially polarized or even, for some choice of parameters, an almost unpolarized beam. Such a property of fractional and deterministic depolarization of fully polarized beams may find some interesting applications in nonlinear photonic devices.

Note that the previously described depolarization property of the NLP does not stand contradiction with its main feature, i.e., the capability to repolarize light. As a matter of fact, the present NLP does not act as a perfect polarizer, in the sense that it only pulls input SOPs toward the vicinity of some point, but not exactly to a given point on the Poincaré sphere. As we shall see in the next subsection, this particular NLP would transform initially unpolarized light into a partially polarized beam with $\text{DOP} = 0.74$. This value is the main statistical characteristic of the polarizer. On the other hand, whenever a NLP is fed not by unpolarized light but by fractionally polarized light or even fully polarized light, its performance remains to a large extent unpredictable. Indeed the output DOP may turn out to be larger or substantially less than 0.74, in a manner which sensitively depends on the size and location of the spot of input SOPs on the Poincaré sphere.

In conclusion, we may note that the time scale for reaching a stationary DOP value, as observed in the right panel of Fig. 3, is of an order of magnitude larger than the time required for entering the regime of perfectly periodic oscillations of the Stokes parameters as shown in Fig. 1. The relatively long relaxation time (say, T_D) towards the stationary DOP is related to the fact that its value is virtually independent of the initial polarization states of the beams. From our simulations we estimate that T_D is typically equal to $100T_{NL}$. In statistics, processes with time-invariant mean values are characterized as stationary. In all our numerical studies we employed relatively long observation times, in order to make sure that the long-term dynamics of the

average values does not depend on time, as we are only dealing here with stationary processes.

3.B. Response to unpolarized light

Let us study now the response of a fiber NLP when fed with unpolarized light at its input. In order to numerically simulate a unpolarized signal, we replace the previously considered stationary boundary conditions at $z = 0$ with the time-varying polarization state as specified by Eqs. (7)-(11). Quite interestingly, as we shall see the repolarization capabilities of the NLP sensitively depend upon the relative value of the input signal modulation frequency ω_m and what can be defined as the cutoff frequency of the NLP response, or $\omega_c = T_{NL}^{-1}$. Just as for the case that was illustrated in Fig. 1, a time interval of the order of a dozen units of T_{NL} is typically enough for reaching an equilibrium (either periodic in time, or stationary) state for the Stokes parameters of the signal and pump beams across the entire fiber. Therefore whenever the input signal polarization modulation frequency is smaller than the NLP cutoff frequency (i.e., $\omega_m T_{NL} \ll 1$) one obtains that the response of the NLP is quasi-stationary. In this situation at any instant of time the pump and signal beams along the fiber are in equilibrium with each other. Such an equilibrium distribution of polarization states is what we call polarization attractor. In our study we are going to deal with both stationary and time-periodic polarization attractors.

In the Approach S (dealing with averaging the response of the NLP over scrambled

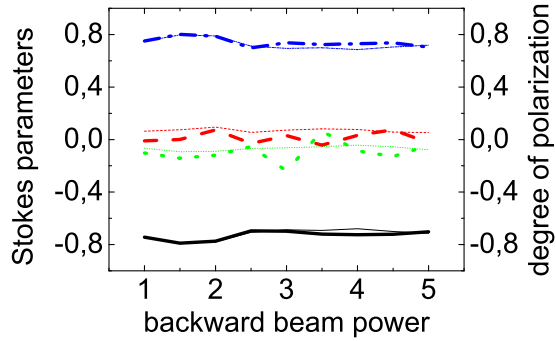


Fig. 4. Components of the mean Stokes vector and the DOP of the output signal beam as a function of the relative power of the pump beam: S_1^+ (black solid); S_2^+ (red dashed); S_3^+ (green dotted), DOP (blue dot-dashed), for the input SOP of the pump beam: (0.99, 0.1, 0.1). Thick (thin) lines are calculated with Approach S(U). The Stokes parameters are normalized with respect to $S_0^+(z, t)$. The observation time in Approach U is $T = 50\omega_m^{-1} = 250000T_{NL}$ and $\omega_m T_{NL} = 0.0002$. The observation time in Approach S is $T = 10000T_{NL}$ and $N = 110$.

beams) the output SOP of each signal beam from the ensemble was detected long after all transient processes have died away and an equilibrium state (i.e., independent of initial conditions) was established for both the signal and the pump beams. Thus, in both the Approach S with detection times $T \gg T_{NL}$ on the one hand, and the Approach U considered in the limit of $\omega_m T_{NL} \ll 1$ and observation times $T > \max(50\omega_m, T_D)$ (these conditions are necessary for modeling the unpolarized beam at the input and at the same time obtaining the long-term value of its output DOP) on the other hand, we are going to deal with equilibrium states for beams inside the fiber. Also, in both approaches we are going to scan the input SOPs across the entire Poincaré sphere. Thus, we may expect that the statistical averages computed with either the Approach S or U are going to be identical. By statistical averages we mean the average values of the three Stokes parameters of the signal and its DOP. Fig. 4 shows that the results of the two approaches are indeed relatively close to each other: the small discrepancies may be attributed to statistical fluctuations. The details of the statistical data processing for Approach S are presented in Appendix A.

The mean values of the Stokes vector components in the Approach U are simply computed as the time averages

$$\langle S_i^+(L, T) \rangle_T = \frac{1}{T} \int_0^T dt S_i^+(L, t), \quad (13)$$

with $i = 1, 2, 3$. Next the DOP is computed as given by Eq. (12): the value shown in

Fig. 4 is exactly the long-term $DOP = 0.74$ (for $S_0^- = 3S_0^+$) for initially unpolarized beams which was mentioned in the previous subsection.

Let us come back from the comparison of Approaches S and U to consider the Approach U in more details. For example, we may observe the temporal dynamics of the output S_1^+ Stokes component of the signal at $z = L$ whenever its input SOP changes adiabatically (i.e., $\omega_m T_{NL} \ll 1$). In Fig. 5 we can see that the output first Stokes component is predominantly localized in the lower part of the graph. Indeed, for the pump SOP considered here the average output signal SOP is attracted to the vicinity of the $(-1, 0, 0)$ pole on the Poincaré sphere, see Ref. [3]. However Fig. 5 also shows that some input SOPs leads to strong spikes in the output SOP, indicating that these SOPs are not attracted by the polarizer. Such events are relatively rare. Overall, the output DOP is 0.74. Large excursions of the output SOP from the attraction point can be detrimental whenever they occur in polarization-sensitive telecom links. In order to avoid them, setups with larger values of DOP should be selected, where such spikes are much less likely. For instance, DOP can be as high as 0.99 for polarizers based on high birefringence or spun fibers, see Ref. [7]. Also, in Ref. [3] the DOP= 0.9 was found for polarizers based on the telecom fibers that we study here, whenever the pump beam SOP is in the vicinity of the pole $(0, 0, 1)$ or $(0, 0, -1)$. In this paper we are interested in studying the time-dependent dynamics or transient properties of lossless polarizers, and not in their optimization. Therefore high and low output DOPs are equally good for the present purposes.

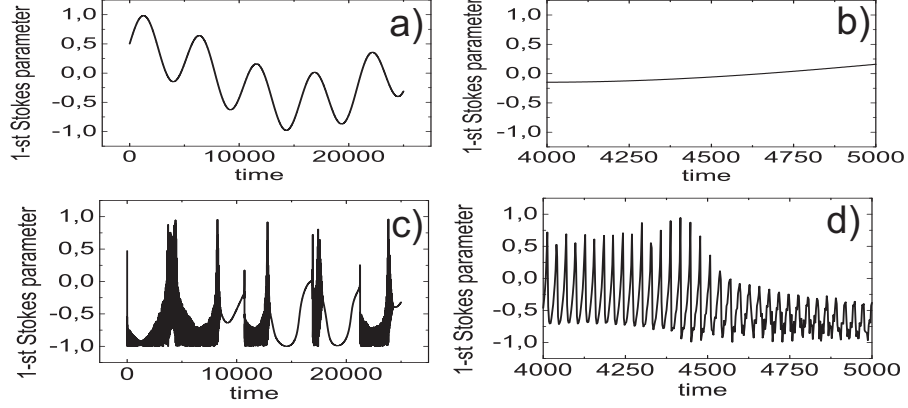


Fig. 5. The 1-st component S_1^+ of the input and output Stokes vector of the signal beam as a function of time: a, b) input; c,d) output. b,d) is the exploded view of a, c). The first Stokes component is normalized with respect to $S_0^+(z, t)$.

The observation time $T = 50\omega_m^{-1}$; $\omega_m T_{NL} = 0.0002$; $S_0^- = 3S_0^+$.

Fig. 5 also demonstrates that for the pump power value $S_0^- = 3S_0^+$ the output signal SOP predominantly exhibits oscillatory behavior, although intervals with a stationary response are also present.

So far we were interested in the adiabatic regime, when $\omega_m T_{NL} \ll 1$ and the counter-propagating beams are in equilibrium at any instant of time. An interesting question is: is the polarizer still effective with higher modulation frequencies, i.e. whenever $\omega_m T_{NL} \sim 1$? In this case signal and pump beams do not have sufficient time to reach an equilibrium state across the fiber. As a consequence, as seen in Fig. 6, the DOP quickly degrades whenever $\omega_m T_{NL}$ approaches unity. Therefore we may conclude that is the presence of a steady-state equilibrium (polarization attractor) between the

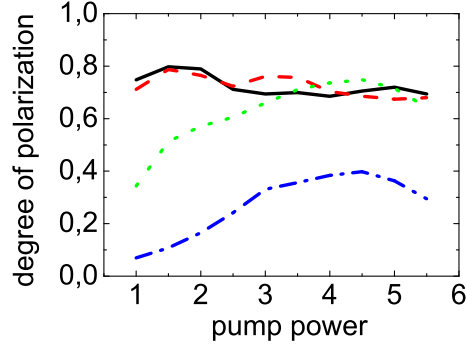


Fig. 6. DOP of the output signal beam as function of the pump power for different values of the product $\omega_m T_{NL}$: 0.0002 (black solid); 0.02 (red dash); 0.2 (green dot); 1 (blue dash-dot). The observation time is $T = 250000T_{NL}$.

signal and pump beams that enables the NLP to work. In other words, signal beam with an input SOP fluctuating faster than T_{NL} will not be effectively repolarized by the polarizer.

In addition to the previous statistical description, it is instructive to study how the polarizer responds to a fast burst of the input signal SOP that is imposed on the otherwise fully polarized signal beam. Such a burst can modeled by imposing a brief disturbance on the angles α_1 and α_2 :

$$\alpha_1 = \alpha_0 + \pi \operatorname{sech} [2.53(\omega_m t - 125)] , \quad (14)$$

$$\alpha_2 = \alpha_0 - \frac{\pi}{2} \operatorname{sech} [3.53(\omega_m t - 125)] , \quad (15)$$

with $\alpha_0 = \pi/4$ and $\omega_m = T_{NL}^{-1}$. Fig. 7 shows that the burst is not compensated by the NLP and it survives the propagation, so that the output Stokes component

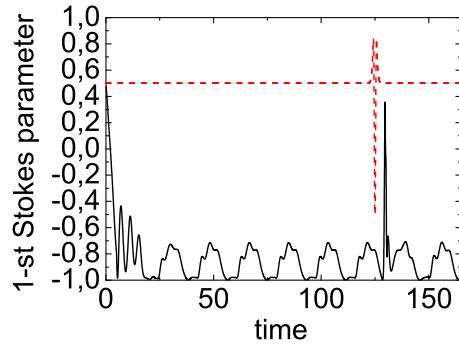


Fig. 7. The first Stokes component of the signal beam at the input (red dash) and output (black solid) of the medium as a function of time. The polarization burst imposed on the otherwise steady-state input SOP is described by Eqs. (14) and (15). $S_0^- = 3S_0^+$.

S_1^+ is disturbed as severely as the input one. However, this disturbance is as brief as the input one. This observation means that the equilibrium state of the signal and the pump beams which is established across the fiber is only locally perturbed and it is immediately recovered after the burst has passed. This resistance to fast perturbation is a natural consequence of the fact that the NLP cannot react faster than its characteristic response time T_{NL} .

In practice, the NLP response time may be controlled by varying the input signal power. Therefore, at least in principle, an input polarization burst of arbitrary short temporal duration (say, T_b) may be always be compensated by the NLP as long as the input signal power becomes sufficiently large (so that $T_b > T_{NL}$). Such situation is

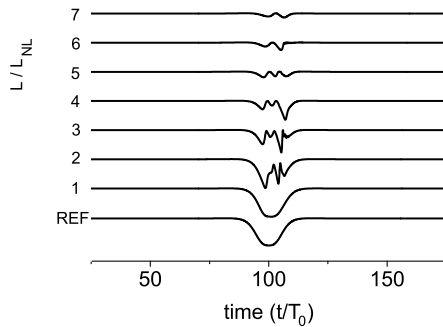


Fig. 8. Illustration of the burst annihilation: The first Stokes component of the signal beam at the output of the medium as the function of time for increasing values of the signal power (from bottom to top). $T_0 = L/v$.

presented in Fig. 8, where we display the output value of S_1^+ parameter as a function of the signal power (measured the number of nonlinear lengths in the total fiber length L). As can be seen, whenever the input signal power is small, the burst propagates through the fiber almost undistorted. However, as the signal power grows larger, the burst is almost entirely annihilated. This compensation is due to shortening of the effective response time T_{NL} , which gradually becomes shorter than the temporal duration of the burst. This plot shows an excellent agreement with the experimental plots presented in section 4 (see Fig. 12).

4. Experimental results

In this section we present an experimental validation of the transient response of the telecom fiber-based NLP which was previously described by means of numerical

simulations. Figure 9 illustrates the experimental setup. The polarization attraction process takes place in a 6.2-km long Non-Zero Dispersion-Shifted Fiber (NZ-DSF). Its parameters are: chromatic dispersion $D = -1.5$ ps/nm/km at 1550 nm; Kerr coefficient $1.7 \text{ W}^{-1}\text{km}^{-1}$; polarization mode dispersion (PMD) $0.05 \text{ ps/km}^{1/2}$. At both ends of the fiber, circulators ensure injection and rejection of the signal (pump). The 0.7 W signal (1.1 W counter-propagating pump) wave consists of a polarized incoherent wave with spectral linewidth of 100 GHz and a central wavelength of 1544 nm (1548 nm). Note that the spectral linewidth of the signal and pump waves is large enough to avoid any Brillouin backscattering effect within the optical fiber. While the pump wave has a fixed arbitrary SOP, a polarization scrambler is inserted to introduce random polarization fluctuations or polarization events in the input signal wave. Finally, the signal is amplified by means of an Erbium doped fiber amplifier (EDFA) before injection into the optical fiber. At the fiber output, the signal SOP is analyzed in terms of its Stokes vectors which is plotted on the Poincaré sphere by means of a polarization analyzer. In order to monitor the polarization fluctuations of the signal wave in the time domain, a polarizer is inserted at port 3 of the circulator before detection by a standard oscilloscope.

Fig. 10 illustrates the polarization attraction efficiency in the S approach. At the input of the fiber, the SOP of the signal randomly fluctuates on a ms-scale by means of the polarization scrambler. That is to say, we inject a set of $N = 128$ beams fully polarized but all with a random SOP. Consequently, on the Poincaré sphere, all the

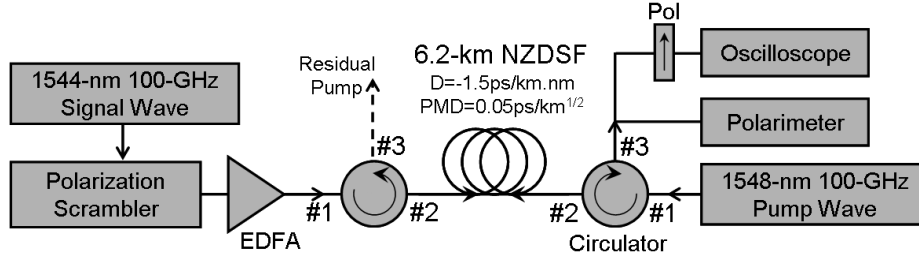


Fig. 9. Experimental setup

points are uniformly distributed on the entire sphere (Fig. 10a). To the opposite, whenever the counter-propagating pump wave is injected (Fig. 10b), we observe an efficient polarization attraction process which is characterized by a small area of output polarization fluctuations, indicating that the SOP of the output signal is efficiently stabilized. The signal DOP is thus increased by the NLP from 0.15 in Fig. 10a to 0.99 in Fig. 10b.

4.A. polarized signal beam

As predicted in the previous section, temporal oscillations or even chaos can be observed during the attraction process in a telecom-fiber-based NLP. Indeed, even if the input signal has a constant SOP and a DOP near unity, closed trajectories can be monitored onto the Poincaré sphere at the output of the NLP, which leads to a slight decrease of the DOP. An example of this phenomenon is presented in Fig. 11. A 700 mW CW input signal, which is fully polarized (DOP= 1) (i.e., no input time fluc-

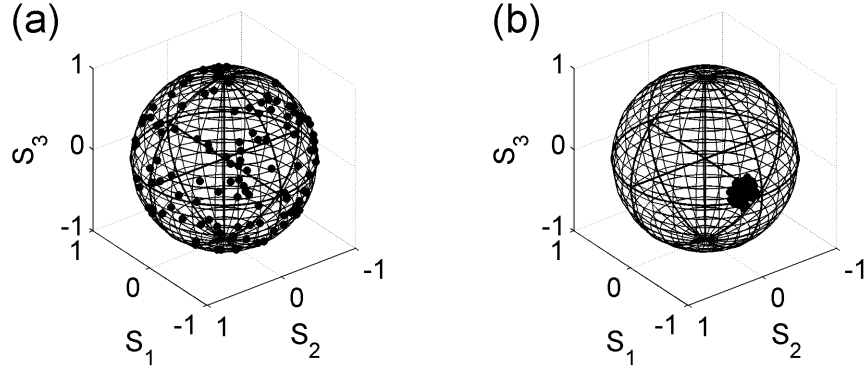


Fig. 10. (a) SOP of the input signal (b) SOP of the output signal

tuations) is injected into the fiber. As can be seen on the Poincaré sphere (Fig. 11a) as well as on Stokes parameters (dashed-lines in Fig. 11c), the input signal SOP is stationary in time. Quite to the opposite, whenever the 1.1 W counter-propagating pump wave is injected into the fiber, a circular-like trajectory can be observed on the signal SOP at the NLP output (Fig. 11b). This corresponds to periodic temporal oscillations of the output signal wave Stokes parameters (Fig. 11c, solid lines). The periodic evolution of S_1^+ , S_2^+ and S_3^+ with a temporal period around $180 \mu\text{s}$, which corresponds to $60 T_{NL}$. We have therefore experimentally confirmed the so far unexpected behavior that a NLP can transform a fully polarized wave into a partially polarized beam with a periodic polarization oscillations, in good agreement with the theoretical predictions of section 3.A.

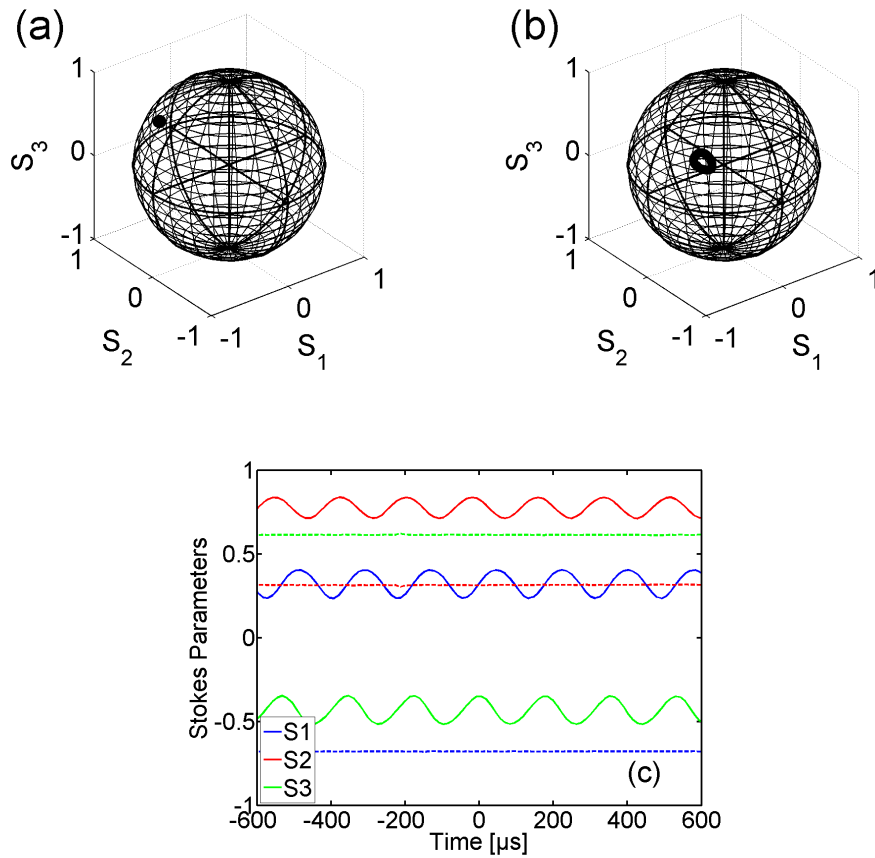


Fig. 11. (a) SOP of the input signal (b) SOP of the output signal (c) Stokes parameters as a function of time (dashed-line input, solid-line output).

4.B. *burst annihilation*

In order to experimentally highlight the transient stage of the attraction process, we recorded the evolution of a fast polarization event as a function of signal power, that is to say as a function of T_{NL} . More precisely, a 30 μ s polarization burst was generated on the signal wave by means of the polarization scrambler. The burst was then injected into the fiber along with the counter-propagating pump wave. At the output of the fiber, we finally detect the burst profile in the time domain thanks to a polarizer. The evolution of the burst is then recorded on both axis of the polarizer as a function of signal power for a constant pump power of 1.1 W. The experimental results are illustrated in Fig. 12.

First of all, we may observe a perfect complementarity between the evolution of the burst of both axis, which provide a general overview of the attraction process. At low signal powers (10 mW), the nonlinear length (55 km) is much longer than the fiber length (6 km), so that no attraction process can be developed. As the signal power is increased, the nonlinear length decreases until it reaches the fiber length for signal powers around 70 mW. At this point, the nonlinear response time T_{NL} is close to the burst duration and the attraction process begins to develop. A transient regime can then be observed with the formation of a short spike on the falling edge of the burst and even slight oscillations, in good agreement with the theoretical predictions of Fig. 8. As the signal power is further increased, the nonlinear length decreases below

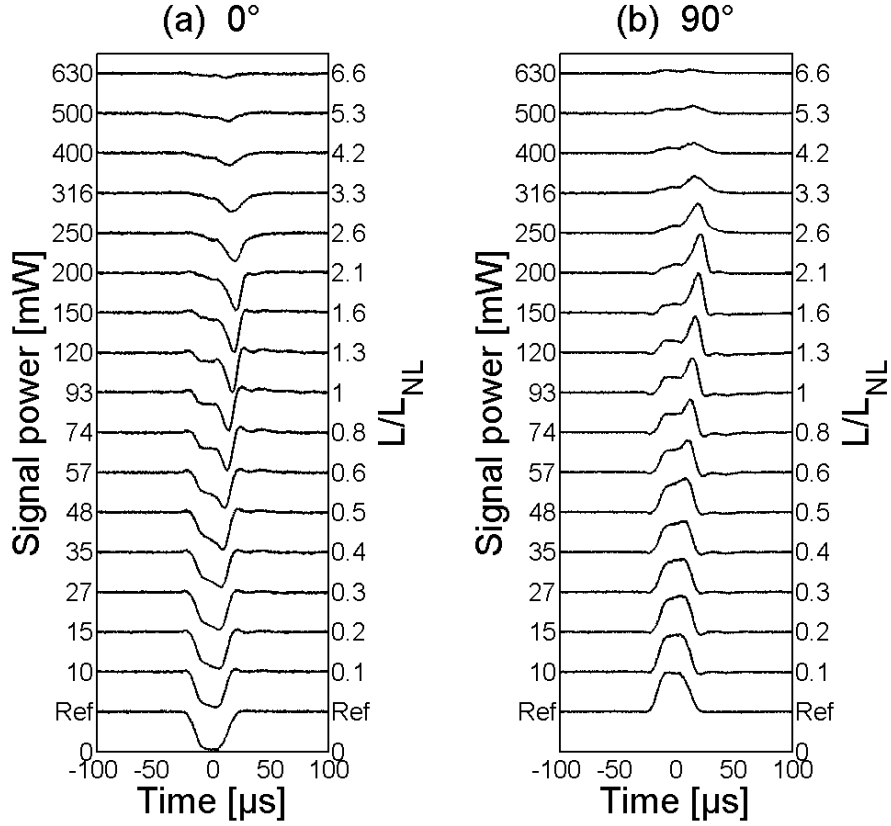


Fig. 12. Evolution of a signal polarization burst as a function of signal average power and detected at the output of the fiber behind a polarizer (a) Along the 0° axis (b) Orthogonal axis.

1 km and the polarization attraction process acts in full strength in order to entirely annihilate the polarization burst.

The previous results are confirmed by calculating the ratio of energy on both axes contained in the polarization burst (Fig. 13). Starting with half of the energy on each component, the attraction process leads to the pulling of 95 % of the entire burst energy on the 0° axis of the polarizer.

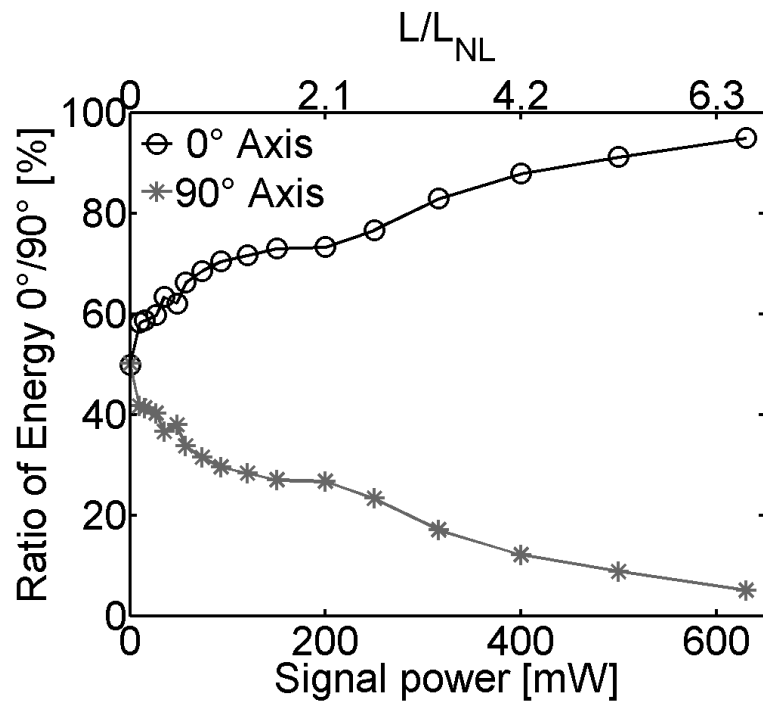


Fig. 13. Ratio of energy on 0°/90° axis contained in the polarization burst.

A similar behavior was also experimentally observed whenever the pump (as opposed to the signal) power was increased. Fig. 14 presents two examples of compensation of a 30 μ s 630 mW polarization burst as a function of pump power. As in Fig. 12, the burst profile was detected at the output of the fiber in the time domain thanks to a polarizer. Once again a transient regime can be observed with the formation of a short spike on the falling edge of the burst. As the pump power increases, around 10 of nonlinear lengths are covered in the fiber, so that the polarization attraction process acts in full strength in order to entirely annihilate the polarization burst.

5. Conclusion

In this paper we studied by both numerical simulations and experiments the transient behavior of telecom fiber-based lossless polarizers. Our main interest is to define the regime for stable long-term behavior of these devices, i.e. when the process of polarization attraction is statistically stationary. In this regime the statistical characteristics of the polarizer (mean SOP and DOP) do not depend on time, therefore represent its universal characteristics. For the polarizer to be in a stationary regime it is sufficient that the observation time is much longer than the average time which characterizes the time scale of fluctuations of the input signal SOP: $\omega_m T \gg 1$.

We found that the most important important time scale to characterize a NLP is its response time T_{NL} . The polarizer exhibits the best performance when fed by signal beams whose input SOPs varies in time slowly with respect to its response time. On

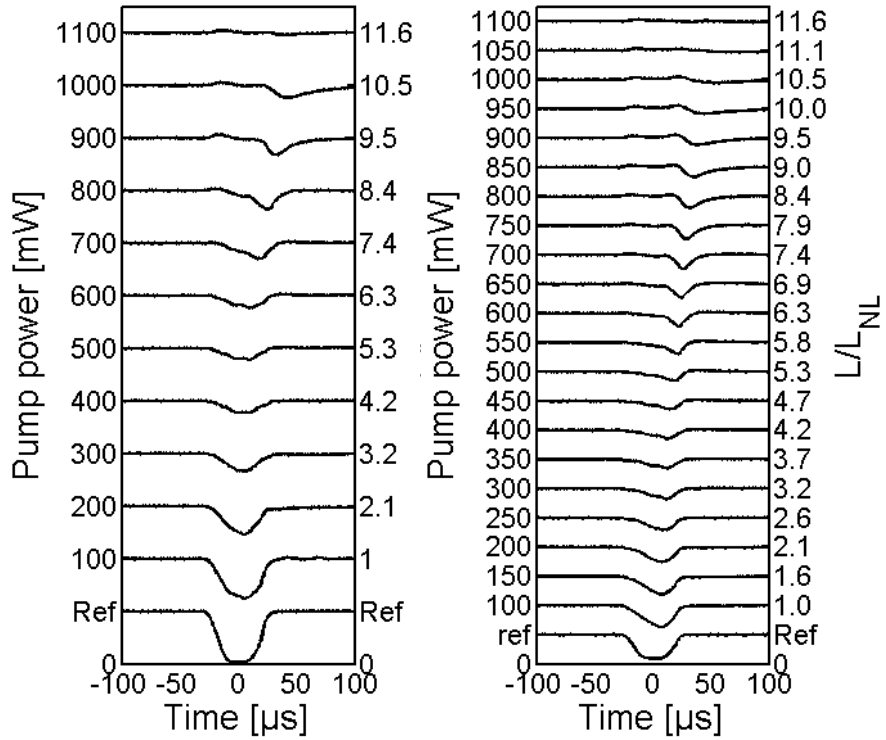


Fig. 14. Two examples of polarization burst evolution as a function of pump power and detected at the output of the fiber behind a polarizer. In distinction to the rest of the paper, here the nonlinear length L_{NL} is defined through the pump power.

the other hand its performance degrades when the rate of fluctuations of input SOP approaches the characteristic response time T_{NL} . For even faster fluctuation rates, the polarizer is no longer able to perform its function.

For signal power around 1 W and typical for telecom fibers nonlinear coefficients $\gamma \sim 1 \text{ (W}\cdot\text{km)}^{-1}$, the nonlinear length $L_{NL} \sim 1 \text{ km}$ and the corresponding response time $T_{NL} \sim 3 \mu\text{s}$. For a nonlinear photonic crystal fiber with $\gamma = 0.1 \text{ (W}\cdot\text{m)}^{-1}$ as used in Ref. [14], the response time can be reduced down to 30 ns. For tellurite photonic crystal fiber with $\gamma = 5.7 \text{ (W}\cdot\text{m)}^{-1}$ as used in Ref. [15], the response time drops below 1 ns. Overall, higher nonlinear coefficients and correspondingly shorter fibers, like that proposed in Refs. [7], are more favorable in applications where the SOP of the signal beam varies faster than $3 \mu\text{s}$.

Acknowledgments

This work was carried out in the frame of the "Scientific Research Project of Relevant National Interest" (PRIN 2008) entitled "Nonlinear cross-polarization interactions in photonic devices and systems" (POLARIZON).

References

1. J. E. Heebner, R. S. Bennink, R. W. Boyd, and R. A. Fisher, "Conversion of unpolarized light to polarized light with greater than 50 efficiency by photorefractive two-beam coupling," *Opt. Lett.* **25**, 257-259 (2000).

2. J. Fatome, S. Pitois, P. Morin, and G. Millot, "Observation of light-by-light polarization control and stabilization in optical fibre for telecommunication applications," *Opt. Express* **18**, 15311-15317 (2010).
3. V. V. Kozlov, J. Nuño, and S. Wabnitz, "Theory of lossless polarization attraction in telecommunication fibers," *J. Opt. Soc. Am. B* **28**, 100-108 (2011).
4. A. Picozzi, "Spontaneous polarization induced by natural thermalization of incoherent light," *Opt. Express* **16**, 17172-17185 (2008).
5. S. Pitois, G. Millot, and S. Wabnitz, "Nonlinear polarization dynamics of counterpropagating waves in an isotropic optical fiber: theory and experiments," *J. Opt. Soc. Am. B* **18**, 432-443 (2001).
6. S. Pitois, J. Fatome, and G. Millot, "Polarization attraction using counterpropagating waves in optical fiber at telecommunication wavelengths," *Opt. Express* **16**, 6646-6651 (2008).
7. V. V. Kozlov and S. Wabnitz, "Theoretical study of polarization attraction in high birefringence and spun fibers," *Opt. Lett.* , to be published (2010).
8. S. Pitois, A. Picozzi, G. Millot, H. R. Jauslin, and M. Haelterman, "Polarization and modal attractors in conservative counterpropagating four-wave interaction," *Europhys. Lett.*, **70**, 8894 (2005).
9. D. Sugny, A. Picozzi, S. Lagrange, and H. R. Jauslin, "Role of singular tori in the dynamics of spatiotemporal nonlinear wave systems," *Phys. Rev. Lett.* **103**,

034102 (2009).

10. E. Assémat, S. Lagrange, A. Picozzi, H. R. Jauslin, and D. Sugny, "Complete nonlinear polarization control in an optical fiber system," *Opt. lett.* **35**, 2025 (2010).
11. S. Lagrange, D. Sugny, A. Picozzi, and H. R. Jauslin, "Singular tori as attractors of four-wave-interaction systems," *Phys. Rev. E* **81**, 016202 (2010).
12. C. Martijn de Sterke, K. R. Jackson, and B. D. Robert, "Nonlinear coupled-mode equations on a finite interval: a numerical procedure," *J. Opt. Soc. Am.* **8**, 403-412 (1991).
13. B. Daino and S. Wabnitz, "Polarization domains and instabilities in nonlinear optical fibers," *Phys. Lett. A* **182**, 289-293 (1993).
14. A. A. Amorim, M. V. Tognetti, P. Oliveira, J. L. Silva, L. M. Bernardo, F. X. Kärtner, and H. M. Crespo, "Sub-two-cycle pulses by soliton self-compression in highly nonlinear photonic crystal fibers," *Opt. Lett.* **34**, 3851-3853 (2009).
15. M. Liao, C. Chaudhari, G.i Qin, Xin Yan, T. Suzuki, and Y. Ohishi, "Tellurite microstructure fibers with small hexagonal core for supercontinuum generation," *Opt. Express* **17**, 12174 (2009).

A. Calculation of the statistics of the Stokes vectors in the Approach S

As explained in the body of the text, for calculating the response of the NLP in the S Approach we used $N = 110$ or 420 signal beams with different SOPs uniformly

distributed over the Poincaré sphere. Then we computed the polarization evolution along the fiber for each of these N realizations, where a pump beam with constant SOP was launched from the opposite end of the fiber. For each realization we measured $S_1^+(L)$, $S_2^+(L)$, and $S_3^+(L)$. At the end of the simulations we calculated the mean values

$$\langle S_i^+(L) \rangle = \frac{1}{N} \sum_{j=1}^N [S_i^+(L)]_j, \quad (16)$$

where $i = 1, 2, 3$. In this form these averages do not define the mean direction of the Stokes vector on the Poincaré sphere, simply because the sum of squares of these means does not yield the square of the power, $(S_0^+)^2$. The length of the vector satisfies the inequality $\sqrt{\langle S_1^+(L) \rangle + \langle S_2^+(L) \rangle + \langle S_3^+(L) \rangle} \leq S_0^+$, and can be even zero for unpolarized light.

However, the information which is contained in the three means is sufficient to restore the direction of the Stokes vector and moreover, to quantify the degree of polarization of the outgoing signal light. The two angles θ_0 and ϕ_0 (called also circular means) which determine the direction of the Stokes vector on the Poincaré sphere are defined as

$$\theta_0 = \arccos \left(\frac{\langle S_3 \rangle}{\sqrt{\langle S_1^+ \rangle^2 + \langle S_2^+ \rangle^2 + \langle S_3^+ \rangle^2}} \right) \quad (17)$$

$$\phi_0 = \text{atan2}(\langle S_2^+ \rangle, \langle S_1^+ \rangle). \quad (18)$$

Here

$$\text{atan2}(x, y) = \begin{cases} \arctan(y/x), & x > 0, \\ \pi + \arctan(y/x), & y \geq 0, x < 0 \\ -\pi + \arctan(y/x), & y < 0, x < 0 \\ \pi/2, & y > 0, x = 0, \\ \pi/2, & y < 0, x = 0 \\ \text{undefined}, & y = 0, x = 0. \end{cases} \quad (19)$$

Finally, the Cartesian coordinates of the Stokes vector are restored as

$$\bar{S}_1 = S_0^+ \sin \theta_0 \cos \phi_0, \quad (20)$$

$$\bar{S}_2 = S_0^+ \sin \theta_0 \sin \phi_0, \quad (21)$$

$$\bar{S}_3 = S_0^+ \cos \theta_0. \quad (22)$$

These values characterize the SOP, while values displayed in the Fig. 4 are simple ensemble averages given by the formulae in Eq. (16).

The degree of polarization is defined as

$$D_S = \sqrt{\langle S_1^+ \rangle^2 + \langle S_2^+ \rangle^2 + \langle S_3^+ \rangle^2} / S_0^+. \quad (23)$$

This is the degree of polarization which is used in the Approach S, and for this reason supplied with index S . Its values are displayed in Fig. 4.